

The effects of zirconia morphology on methanol synthesis from CO and H₂ over Cu/ZrO₂ catalysts Part I. Steady-state studies

Michael D. Rhodes, Alexis T. Bell*

*Chemical Sciences Division, Lawrence Berkeley National Laboratory, and Department of Chemical Engineering, University of California,
Berkeley, CA 94720-1462, USA*

Received 30 December 2004; revised 23 March 2005; accepted 24 April 2005

Available online 31 May 2005

Abstract

The effect of zirconia phase on the activity and selectivity of Cu/ZrO₂ for the hydrogenation of CO was investigated. Relatively pure t-ZrO₂ and m-ZrO₂ were prepared with high surface areas (~145 m²/g). Copper was then deposited on the surface of these materials by either incipient-wetness impregnation or deposition-precipitation. For a fixed Cu surface area, Cu/m-ZrO₂ was ten times more active for methanol synthesis than Cu/t-ZrO₂ from a feed of 3:1 H₂/CO at 3.0 MPa and temperatures between 473 and 523 K. Cu/m-ZrO₂ also exhibited a higher selectivity for methanol. Increasing the Cu surface area on m-ZrO₂ resulted in further improvement in activity with minimal change in selectivity. Methanol productivity increased linearly for both Cu/t-ZrO₂ and Cu/m-ZrO₂ with increasing Cu surface area. The difference in inherent activity of each phase paralleled the stronger and larger CO adsorption capacity of the Cu/m-ZrO₂ as quantified by CO-TPD. The higher CO adsorption capacity of Cu/m-ZrO₂ is attributed to the presence of a high concentration of anionic vacancies on the surface of m-ZrO₂. Such vacancies expose cus-Zr⁴⁺ cations, which act as Lewis acid centers and enhance the Brønsted acidity of adjacent Zr–OH groups. The presence of cus-Zr⁴⁺ sites and adjacent Brønsted acidic Zr–OH groups contributes to the adsorption of CO as HCOO–Zr groups, which are the initial precursors to methanol.

© 2005 Elsevier Inc. All rights reserved.

Keywords: Methanol synthesis; CO; H₂; Cu; ZrO₂

1. Introduction

Zirconia-supported copper exhibits high activity for the synthesis of methanol via hydrogenation of either CO or CO₂, and a broad range of mixtures of CO and CO₂ [1–11]. The latter characteristic is of considerable interest, since conventional Cu/ZnO/Al₂O₃ catalysts operate best over a narrow range of CO₂/CO ratios and, in the absence of traces of H₂O, are virtually inactive for the hydrogenation of pure CO [12]. Mechanistic studies of methanol synthesis over Cu/ZrO₂- and ZrO₂-promoted Cu/SiO₂ have shown

that Cu and ZrO₂ are involved in the synthesis of methanol from CO or CO₂ and H₂ [9]. During CO hydrogenation, CO adsorbs on cus-Zr⁴⁺ Lewis acid sites and interacts with surface hydroxyl groups to generate formate species. These species then undergo sequential hydrogenation to form methoxide species, which are eliminated reductively to form methanol. Cu is more effective at dissociating molecular H₂ than is ZrO₂ [5] and, therefore, provides atomic hydrogen to the surface of ZrO₂ via spillover. This spillover process is facilitated by hydroxyl groups on the ZrO₂ surface [13]. Similar processes take place during the hydrogenation of CO₂, but in this case bicarbonate species are produced initially by the reaction of CO₂ with hydroxyl groups on the surface of ZrO₂, and these species then undergo hydrogenation to form methanol and water.

* Corresponding author.

E-mail address: bell@cchem.berkeley.edu (A.T. Bell).

Since zirconia participates in the hydrogenation of CO over Cu/ZrO₂, the structure of the oxide lattice is expected to influence the performance of such catalysts. Previous studies have shown that the tetragonal (t-ZrO₂) and monoclinic (m-ZrO₂) modifications of ZrO₂ possess different acid/base properties [14–18] and surface hydroxyl group concentrations [17,19]. These characteristics affect the overall uptake of CO and the relative binding of adsorbed species. In a preliminary study of the effects of ZrO₂ phase on the synthesis of methanol, Jung and Bell reported a 7.5-fold higher activity for CO hydrogenation over 5% Cu/m-ZrO₂ than over 5% Cu/t-ZrO₂, and for CO₂ hydrogenation, the activity was 4.5 times higher on the former catalyst [11]. The effects of the zirconia phase have also been noted in studies of the isosynthesis of isobutene and higher alcohols [20,21] and butane isomerization [22]. Given the role of Cu as a source of hydrogen atoms, the surface area of Cu is also expected to influence the catalytic activity of CO hydrogenation. Although previous studies have shown a linear relation between Cu surface area and methanol synthesis activity for CO₂-containing feeds [23–25], there is a need to understand how this parameter affects the rate of methanol formation in the absence of CO₂.

The objective of the present investigation was to determine the effects of the ZrO₂ phase on the activity and selectivity of ZrO₂-supported Cu for methanol synthesis from CO and H₂. The influence of the Cu deposition method and the surface area of the deposited Cu were also examined. The phase of the supports was identified by XRD and Raman spectroscopy, and N₂O titration was used to determine the surface area of the dispersed Cu. The CO chemisorption capacity of the catalyst was probed by temperature-programmed desorption spectroscopy, and the nature of the hydroxyl groups present on ZrO₂ was examined by infrared spectroscopy. This paper constitutes the first of a two-part series and is devoted to defining and interpreting the effects of the ZrO₂ phase and the Cu surface area on the steady-state activity and selectivity of Cu/ZrO₂ catalysts for methanol synthesis from H₂ and CO. The second part of this series examines the dynamics of methanol synthesis by in situ infrared spectroscopy and attempts to provide additional insight into the manner by which the ZrO₂ phase and the Cu surface area affect the rates of elementary processes involved in the hydrogenation of CO to methanol.

2. Experimental

2.1. Catalyst preparation

Details of the synthesis of monoclinic and tetragonal zirconia used for this study have been described previously [26]. We prepared a low-pH, hydrous ZrO₂ (ZrO₂ (LpH)) by boiling a 0.5 M solution of zirconyl chloride (ZrOCl₂·8H₂O, 99.99%; Aldrich) under reflux at 378 K for 240 h. The final solution had a pH < 1. NH₄OH was added dropwise to ag-

glomerate the resulting fine particles to facilitate their filtration. The recovered precipitate was washed and redispersed in deionized water several times to remove residual chlorine. AgNO₃ was used to test the filtrate for any remaining Cl anions. The material was then dried in air at 383 K overnight before calcination. A high-pH, hydrous ZrO₂ (ZrO₂ (HpH)) was prepared by dropwise addition of a 1 M ammonium hydroxide solution to a 0.5 M solution of zirconyl chloride at a pH of 10. The resulting material was heated in the mother liquor at 378 K under reflux for 240 h while the pH was maintained at 10. The precipitated material was washed and dried in a fashion similar to that used for the low-pH sample. Each sample was calcined in dry air flowing at 100 cm³/min. The temperature was ramped from room temperature at a rate of 2 K/min to the final temperature, which was maintained for 3 h.

Cu/ZrO₂ catalysts were prepared by both incipient-wetness impregnation and deposition-precipitation. We carried out incipient-wetness impregnation by dissolving the desired amount of copper nitrate (Cu(NO₃)₂·6H₂O, 99.999% metals basis; Alfa Aesar) in a volume of deionized water sufficient to fill the pore volume of the ZrO₂ support. This solution was then mixed with the ZrO₂ and left to dry under mild heating (~313 K) for > 120 h, before it was dried at 383 K overnight. Samples prepared in this fashion are designated with the suffix (I). We carried out deposition-precipitation by immersing the ZrO₂ support in an aqueous solution of copper nitrate that was stirred vigorously [27]. The ratio of support to solution was 0.5 g/60 cm³. We slowly raised the pH by injecting a solution of NaOH with a motor-driven syringe inserted through a septum seal located near the bottom of the preparation vessel. The rate of base addition was set at 1 OH⁻/Cu²⁺ h for each Cu loading. The addition of base was discontinued once the pH of the solution reached approximately 7.3. Samples prepared in this fashion are designated with the suffix (DP).

Before testing or characterization, each catalyst sample (0.15 g) was calcined in a 10% O₂/He mixture flowing at 60 cm³/min. The sample was heated from room temperature to 573 K at 0.5 K/min and then maintained at 573 K for 2 h. The sample was then cooled to 323 K, swept with He, and then reduced in a 10% H₂/He mixture flowing at a rate of 60 cm³/min while the temperature was increased at a rate of 2 K/min to 573 K. The flow of 10% H₂/He was maintained at 573 K for 1 h before the flow was switched to 100% H₂ for an additional hour.

2.2. Catalyst characterization

The crystallographic phase of each material was determined by both X-ray diffraction and Raman spectroscopy. XRD patterns were obtained with a Siemens D5000 diffractometer, which uses Cu-K_α radiation and a graphite monochromator. Scans were made in the 2θ range of 20°–45° with a step size of 0.02° and a time step of 11 s. The volume fraction of the monoclinic phase, V_m, of each sample was

calculated from the following relationships [28]:

$$V_m = \frac{1.311X_m}{1 + 0.311X_m},$$

$$X_m = \frac{I_m(111) + I_m(11\bar{1})}{I_m(111) + I_m(11\bar{1}) + I_t(111)},$$

where $I_m(111)$ and $I_m(11\bar{1})$ are the line intensities of the (111) and (11 $\bar{1}$) peaks for m-ZrO₂ and $I_t(111)$ is the intensity of the (111) peak for t-ZrO₂. Raman spectra were recorded with a HoloLab 5000 Raman spectrometer (Kaiser Optical) at room temperature. The stimulating light source was a Nd:YAG laser, the output of which is frequency doubled to 532 nm. Laser power at the sample was approximately 20 mW.

The BET surface area of each ZrO₂ material was determined with an Autosorb gas adsorption system with nitrogen adsorption/desorption isotherms. Before each analysis, samples were dried at 393 K under vacuum for > 2 h. BET surface areas were calculated with the use of a 5-point isotherm.

Cu surface areas were quantified with N₂O titrations followed by H₂-TPR to account for any potential bulk oxidation effects [29]. The sample (0.15 g) was calcined (10% O₂/He) and reduced (2% H₂/He) in a flow microreactor heated by a furnace. The temperature was measured with a thermocouple placed inside the catalyst bed from above. Reduced samples were cooled to 333 K and then exposed to 1% N₂O/He for varying times, followed by rapid cooling to 298 K in He. Neither of the ZrO₂ supports exhibited a significant interaction with N₂O at this temperature. We then performed H₂-TPR by ramping the temperature up to 673 K at a rate of 20 K/min under 0.2% H₂/He flowing at a rate of 60 cm³/min. The amount of H₂ consumed was used to calculate the amount of oxygen deposited after the N₂O titration. A total of 1.46×10^{19} Cu atoms/m² and a stoichiometry of 2 Cu/H₂ were used [30]. No significant bulk oxidation was observed for any of the catalyst samples.

The concentration of exchangeable hydrogen on each sample was quantified by H/D exchange. Fully reduced samples were purged with He at 298 K for 30 min, followed by ramping of the temperature at 20 K/min from 298 to 623 K in 40 cm³/min of D₂. Both HD and H₂ evolution were monitored with a mass spectrometer, but only HD generation was observed. For each sample, exchange was complete by ~ 523 K.

Transmission infrared spectroscopy experiments were conducted with a low dead volume infrared cell with CaF₂ windows [31]. In an effort to remove any residual surface species before testing, each sample was calcined in a 10% O₂/He mixture flowing at 60 cm³/min. The sample was heated from room temperature to 523 K at 2 K/min and then maintained at 523 K for 8 h. The sample was then cooled to 323 K, swept with He, and then reduced in a 10% H₂/He mixture flowing at a rate of 60 cm³/min, and during reduction the temperature was increased at the rate of 2 K/min to 523 K. The flow of 10% H₂/He was maintained at 523 K for

1 h before the flow was switched to 100% H₂ for an additional 1–3 h. The sample was then flushed with He for 1 h before spectrum collection.

H₂-TPR studies were conducted with 0.15 g of a calcined sample purged with He at 298 K for 30 min. The flow was then switched to 2% H₂/He at a flow rate of 60 cm³/min and then ramped from 298 to 673 K while we monitored H₂ consumption with a mass spectrometer.

CO adsorption of the catalysts was determined by temperature-programmed desorption (TPD). The sample was first calcined and reduced, after which it was cooled to 523 K and flushed with He for 30 min. CO/He (4.0%) was then passed over the catalyst at a rate of 60 cm³/min for 20 min. The sample was then cooled to 298 K in 4.0% CO/He before being purged with He to remove any weakly adsorbed species. We studied desorption by ramping the temperature at 20 K/min in He from 298 to 773 K while monitoring the desorbing gas with a mass spectrometer.

2.3. Catalyst testing

Activity and selectivity measurements for CO hydrogenation were carried out in a continuous-flow, fixed-bed reactor. The stainless-steel reactor tube had an internal fused glass lining with a 4.0-mm ID (SGE). The temperature was measured with a thermocouple inserted in the catalyst bed with a metal sheath. Reactant gas mixtures of CO (99.99%) and 99% H₂/Ar (99.99%) were further purified with appropriate traps to remove H₂O, CO₂, and O₂. CO was passed through a trap filled with glass bead and heated to 673 K to decompose iron carbonyl formed in the CO cylinder. Flow rates were controlled with high-pressure, mass-flow controllers (Brooks), and the total pressure was regulated with a back-pressure regulator (Go). The exit line from the reactor to the gas-sampling valve was heated to prevent condensation of any volatile products. Product gas mixtures were analyzed with a gas chromatograph equipped with both a TCD and a FID (HP 6890).

Reactions were carried out with 0.15 g of catalyst. The feed was a 3:1 H₂/CO mixture flowing at a rate of 60 cm³/min STP. The total pressure maintained in the reactor was 3.0 MPa. The composition of the products was analyzed after 2 h on stream at a given temperature. The temperature was then raised to the next temperature at a rate of 2 K/min and then held constant for an additional 2 h. Conversion and selectivity were determined on the basis of CO, the limiting reactant.

3. Results

3.1. Characterization of ZrO₂ supports

Given the difference in preparation of the high-pH and low-pH forms of ZrO₂, the product from each synthetic approach was calcined at a different temperature to obtain ma-

materials with essentially equivalent surface areas. The calcination temperature and measured surface area for each support are given in Table 1. To achieve surface areas of $\sim 145 \text{ m}^2/\text{g}$, it was necessary to calcine ZrO_2 (HpH) at a higher temperature than ZrO_2 (LpH). XRD patterns for these materials are shown in Fig. 1. The bulk monoclinic volume fraction (V_m) was $> 99\%$ for ZrO_2 (LpH) and $< 3\%$ for ZrO_2 (HpH).

The Raman spectra of the zirconia supports are presented in Fig. 2. ZrO_2 (HpH) exhibits multiple peaks at 157, 280, 321, 472, and 646 cm^{-1} . The positions of these peaks and

the higher intensity of the peak at 646 cm^{-1} compared with that at 472 cm^{-1} are all characteristic of t- ZrO_2 [32–34]. ZrO_2 (LpH) exhibits peaks at 182, 333, 377, 475, 559, and 623 cm^{-1} , which are characteristic of m- ZrO_2 [32–34]. These observations are consistent with those of XRD analysis and confirm that ZrO_2 (HpH) and ZrO_2 (LpH) are relatively pure samples of t- ZrO_2 and m- ZrO_2 , respectively. For ease of reference, ZrO_2 (HpH) will be referred to as t- ZrO_2 and ZrO_2 (LpH) will be referred to as m- ZrO_2 .

3.2. Characterization of 1.2% Cu/t- ZrO_2 and 1.2% Cu/m- ZrO_2

A loading of 1.2 wt% Cu was deposited on each support in order to identify the effects of support morphology and Cu deposition procedure on the Cu dispersion and, ultimately, on the methanol synthesis activity of Cu/ ZrO_2 . The Cu surface area and associated dispersion for each sample are given in Table 2. In all cases, deposition-precipitation generates a larger copper surface area than incipient-wetness impregnation. In addition, for a given Cu-deposition technique, the Cu dispersion is higher on t- ZrO_2 than on m- ZrO_2 . This result can be attributed to the higher point of zero charge (PZC) (8.5 vs. 6.6–6.7) and charge density of the monoclinic polymorph [19]. The larger net positive charge at the surface of m- ZrO_2 leads to a weaker interaction between the support and the dissolved Cu cations, which contributes to a lower dispersion.

The surface concentration of exchangeable hydrogen, quantified by H/D exchange, for each sample is also listed in Table 2. Previous studies have shown that this quantity is indicative of the concentration of hydroxyl groups on the catalyst surface [13,35]. The concentration of OH groups ranges from 6.3 to $10.9 \mu\text{mol}/\text{m}^2$; this is about 50% higher on Cu/m- ZrO_2 than it is on Cu/t- ZrO_2 . A similar trend has been reported for pure ZrO_2 [26].

Infrared spectra for the O–H stretching region for t- ZrO_2 and m- ZrO_2 are shown in Fig. 3. Spectra were referenced to the empty cell in He. Each sample exhibits two types of isolated hydroxyl groups in the region above 3600 cm^{-1} . For t- ZrO_2 these peaks occur at 3660 and 3738 cm^{-1} , and for m- ZrO_2 the peaks occur at 3668 and 3729 cm^{-1} . Although several authors have noted the presence of a pair of OH bands on t- ZrO_2 and m- ZrO_2 [36–38], their exact position has been found to depend on the degree of surface dehydroxylation. Of notable interest is the work of Erkelens

Table 1

Preparation calcination temperature and textural characteristics for each ZrO_2 material

Sample	Calcination temperature (K)	Surface area ($\text{m}^2/\text{g}_{\text{cat}}$)	Avg. pore size (nm)
ZrO_2 (HpH)	1053	150	4.2
ZrO_2 (LpH)	738	143	4.1

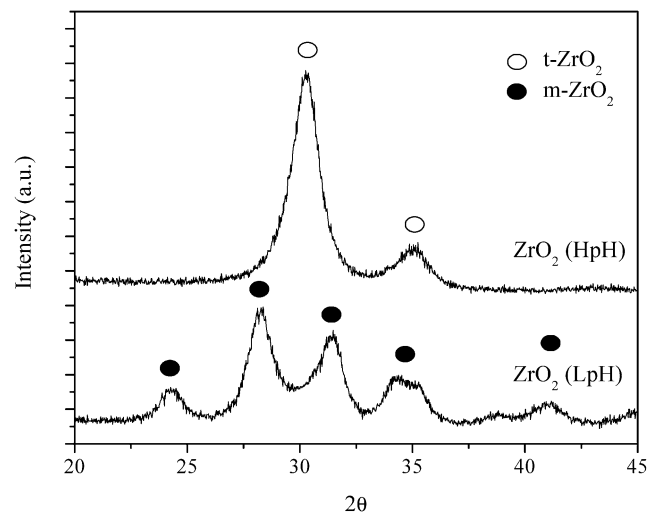


Fig. 1. XRD patterns for ZrO_2 (HpH) and ZrO_2 (LpH).

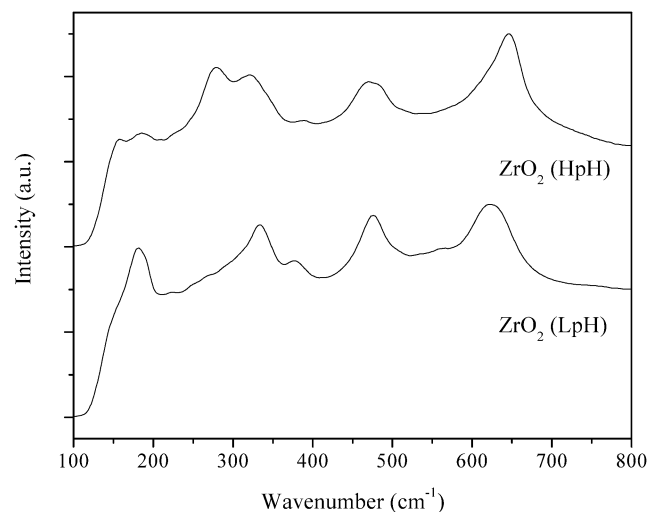


Fig. 2. Raman spectra for ZrO_2 (HpH) and ZrO_2 (LpH) taken at room temperature.

Table 2

Effect of ZrO_2 phase on the dispersion of Cu and exchangeable H for 1.2 wt% Cu/ ZrO_2 catalysts

Sample	Cu surface area ($\text{m}^2/\text{g}_{\text{cat}}$)	Cu dispersion (%)	Exchangeable H ($\mu\text{mol}/\text{m}^2$)
1.2 wt% Cu/t- ZrO_2 (I)	0.93	11.9	7.9
1.2 wt% Cu/t- ZrO_2 (DP)	1.44	18.5	6.3
1.2 wt% Cu/m- ZrO_2 (I)	0.58	7.4	10.7
1.2 wt% Cu/m- ZrO_2 (DP)	0.87	11.1	10.9

et al. [36], who observed OH bands very similar to those reported here for samples of t-ZrO₂ and m-ZrO₂ prepared and calcined in a manner very similar to that used here. Hydroxyl group species on the surface of ZrO₂ are commonly assigned based on the number of coordinating Zr cations; the higher frequency species represent terminal groups and the lower frequency species represent either bi- or tribridging groups [37,39]. Recent theoretical studies of the surfaces of both ZrO₂ polymorphs have also led to the conclusion that a combination of terminal and both bi- and tribridged OH groups should be present [40–43]. Under the conditions of this study, m-ZrO₂ exhibits a higher relative concentration of the lower frequency hydroxyl group species.

The H₂-TPR profile for each catalyst is given in Fig. 4. All of the samples of 1.2 wt% Cu exhibit peaks between 473 and 573 K. Previous authors have observed similar reduction peaks for Cu/ZrO₂ and have attributed the lower temperature peaks to the reduction of highly dispersed CuO or Cu²⁺ ions in an octahedral environment, whereas the high-temperature peak at 573 K has been attributed to the reduction of bulk CuO [44,45]. Even though the dispersion of Cu on m-ZrO₂ is lower than that on t-ZrO₂, it reduces at a significantly lower temperature. Reduction is also easier for Cu deposited by deposition-precipitation. For each catalyst, however, the amount of H₂ consumed was slightly greater than the value corresponding to the complete reduction of CuO species (H₂/CuO ~ 1.0–1.1). Therefore, Cu should exist predomi-

nantly as Cu⁰ regardless of the ZrO₂ phase or method of Cu deposition sample during reaction, after pre-reduction up to 573 K. Previous investigators have noted H₂ consumption peaks associated with the reduction of ZrO₂ at $T > 673$ K [44,46]. Such peaks were not observed in the present study because the reduction temperature was limited to ≤ 673 K.

TPD spectra taken after the adsorption of CO at 523 K are shown in Fig. 5 for 1.2 wt% Cu/t-ZrO₂ (DP) and 1.2 wt% Cu/m-ZrO₂ (DP) (the corresponding samples in which Cu was deposited by impregnation are not shown). Each material desorbed the adsorbed CO as both CO and CO₂. The desorption of CO and CO₂ has previously been ascribed to the decomposition of formate and carbonate species, respectively [17]. The significantly greater CO adsorption capacity of Cu/m-ZrO₂ is quite apparent. It is also noted that CO and CO₂ desorption occurs at higher temperatures for m-ZrO₂, indicating a stronger binding of adsorbed CO to the surface of this material. Based on total carbon adsorption, the Cu-containing materials exhibited CO adsorption capacities similar to those reported for t-ZrO₂ and m-ZrO₂ free of Cu [17]. The calculated desorption quantities and related peak maxima temperatures for all of the samples are listed in Table 3. In general, the impregnated materials exhibit desorption spectra that are similar to those for the corresponding materials prepared by deposition-precipitation, but with lower overall adsorption capacities.

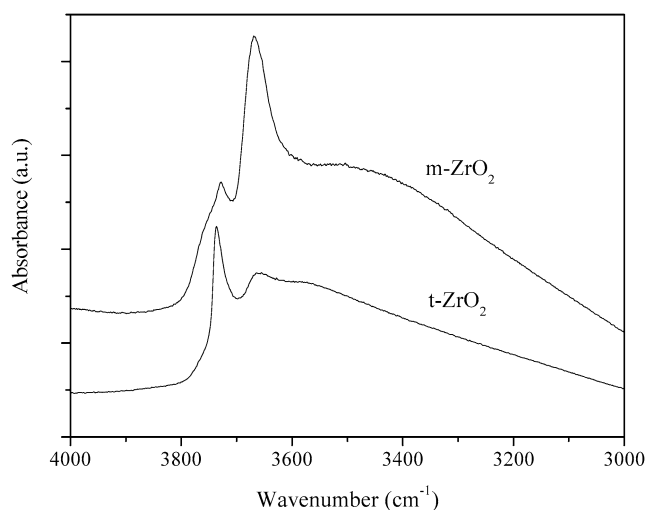


Fig. 3. Infrared spectra of the hydroxyl group stretching region for t-ZrO₂ and m-ZrO₂.

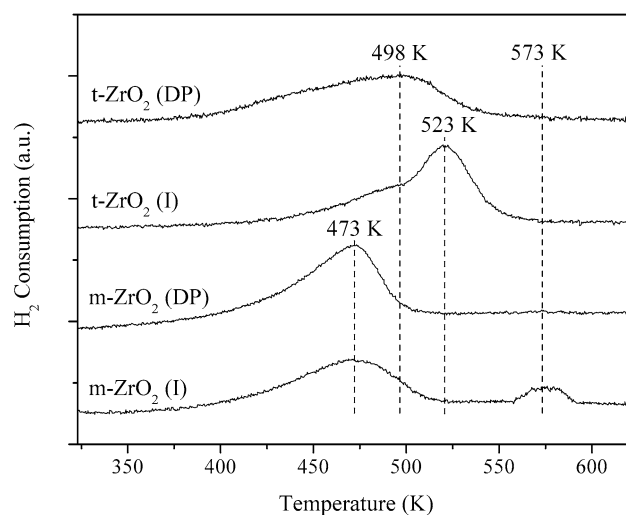


Fig. 4. H₂-TPR spectra for 1.2 wt% Cu deposited on t-ZrO₂ and m-ZrO₂ by deposition-precipitation (DP) and by incipient-wetness impregnation (I). Heating rate = 20 K/min; 2% H₂/He flow rate = 60 cm³/min.

Table 3
Effect of ZrO₂ phase on the adsorption capacity and binding strength of CO at 523 K

Sample	CO desorbed (μmol/m ²)	Peak max. T (K)	CO ₂ desorbed (μmol/m ²)	Peak max. T (K)	Total CO _x desorbed (μmol/m ²)
1.2 wt% Cu/t-ZrO ₂ (I)	0.01	440	0.03	425, 605	0.04
1.2 wt% Cu/t-ZrO ₂ (DP)	0.01	440	0.05	435, 595	0.06
1.2 wt% Cu/m-ZrO ₂ (I)	0.26	635	0.61	585, 640	0.87
1.2 wt% Cu/m-ZrO ₂ (DP)	0.51	620	0.78	590, 675	1.29

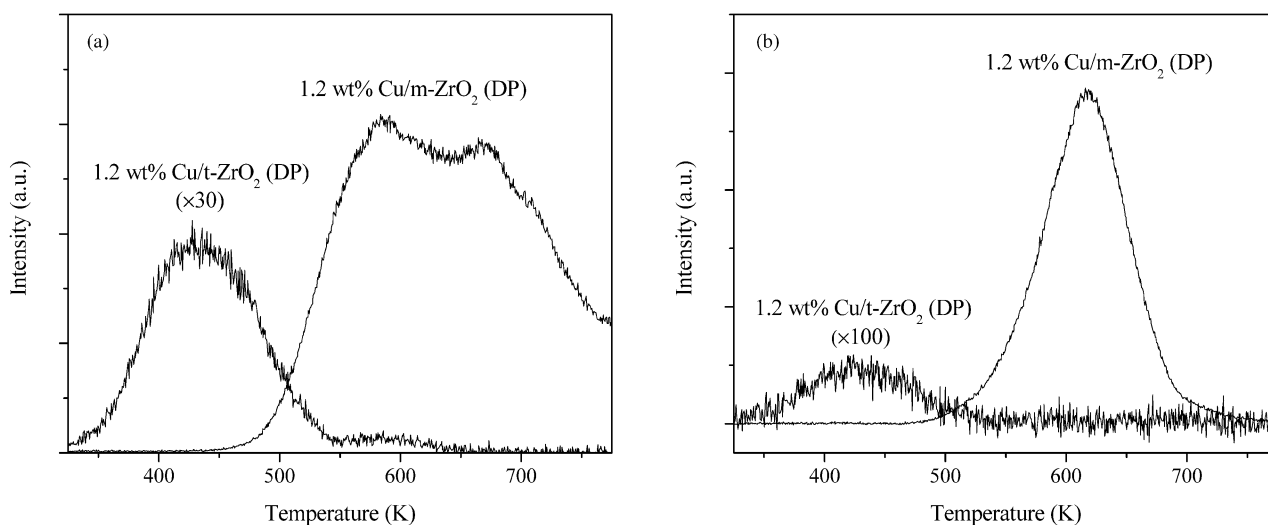


Fig. 5. TPD spectra of (a) CO₂ and (b) CO following CO adsorption on 1.2 wt% Cu/t-ZrO₂ (DP) and 1.2 wt% Cu/m-ZrO₂ (DP). Heating rate = 20 K/min; He flow rate = 60 cm³/min.

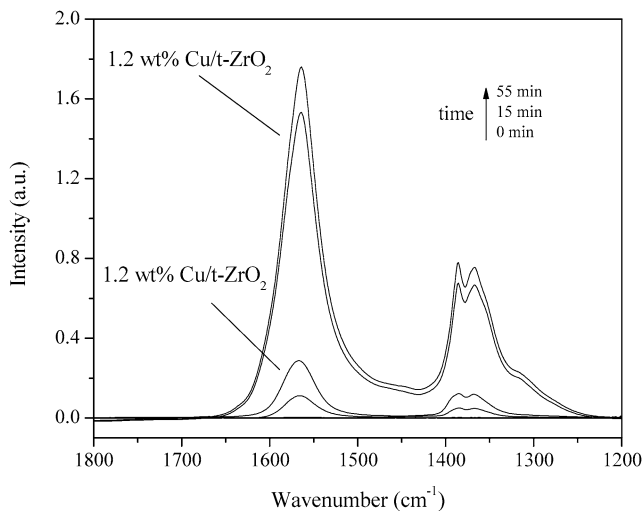


Fig. 6. Infrared spectra of 1.2 wt% Cu/t-ZrO₂ (DP) and 1.2 wt% Cu/m-ZrO₂ (DP) at 523 K after switching from 0.50 MPa He to 0.05 MPa CO and 0.45 MPa He flowing at a total flow rate of 60 cm³/min. Spectra referenced to 1.2 wt% Cu/t-ZrO₂ (DP) and 1.2 wt% Cu/m-ZrO₂ (DP) obtained in 0.50 MPa He flowing at 523 K.

To establish the form in which CO adsorbs to Cu/ZrO₂, in situ infrared spectra were taken during CO adsorption on the reduced catalysts. Fig. 6 shows a sequence of spectra obtained after exposure of 1.2 wt% Cu/t-ZrO₂ (DP) and 1.2 wt% Cu/m-ZrO₂ (DP) to a flow containing 0.05 MPa CO and 0.45 MPa He at 523 K. The adsorption intensities for bidentate formate species on ZrO₂ (1566, 1386, and 1366 cm⁻¹) [9,17,47–53] are large for each sample but are significantly greater for the m-ZrO₂ catalyst, consistent with the higher adsorption capacity measured by TPD. The evolution of these bands illustrates that CO adsorption is incomplete after 20 min and that the dynamics of formate formation are slower on 1.2 wt% Cu/t-ZrO₂. Therefore, the large adsorption capacity differences measured with TPD are to

some extent a reflection of the more rapid generation of formate species on the m-ZrO₂ surface.

3.3. Catalytic performance of low weight loaded Cu/t-ZrO₂ and Cu/m-ZrO₂

The effects of reaction temperature on the activity and selectivity of 1.2 wt% Cu/ZrO₂ catalysts are presented in Fig. 7. The conversion of CO to methanol increased over the temperature range of 473–523 K and was accompanied by a decrease in methanol selectivity. The only major by-product observed was methane. The reported conversions are far below the equilibrium values for the given temperatures, which means that the observed rate of methanol formation is not influenced significantly by methanol decomposition. Both m-ZrO₂-supported catalysts exhibited significantly higher conversions to methanol than the t-ZrO₂-supported catalysts. For example, the methanol productivity of 1.2 wt% Cu/m-ZrO₂ (DP) was approximately eight times higher than that of 1.2 wt% Cu/t-ZrO₂ (DP) at 523 K. The higher activity of the m-ZrO₂-supported catalysts was accompanied by a substantially greater selectivity for methanol. It is also noted that introduction of Cu by deposition-precipitation yielded higher conversions and selectivities than could be achieved by the introduction of Cu by incipient-wetness impregnation, regardless of the phase of ZrO₂.

3.4. Effects of Cu loading on the properties of Cu/m-ZrO₂

Table 4 presents the copper surface areas, copper dispersion, and the surface concentration of exchangeable hydrogen measured for Cu/m-ZrO₂ containing 1.2–20 wt% Cu. Since deposition-precipitation produces a higher dispersion of Cu, these catalysts were prepared with this technique. Although increasing the copper loading decreases the Cu dispersion, the total Cu surface area increases to 10 wt% before decreasing for 20 wt% Cu/m-ZrO₂ (DP). The increase

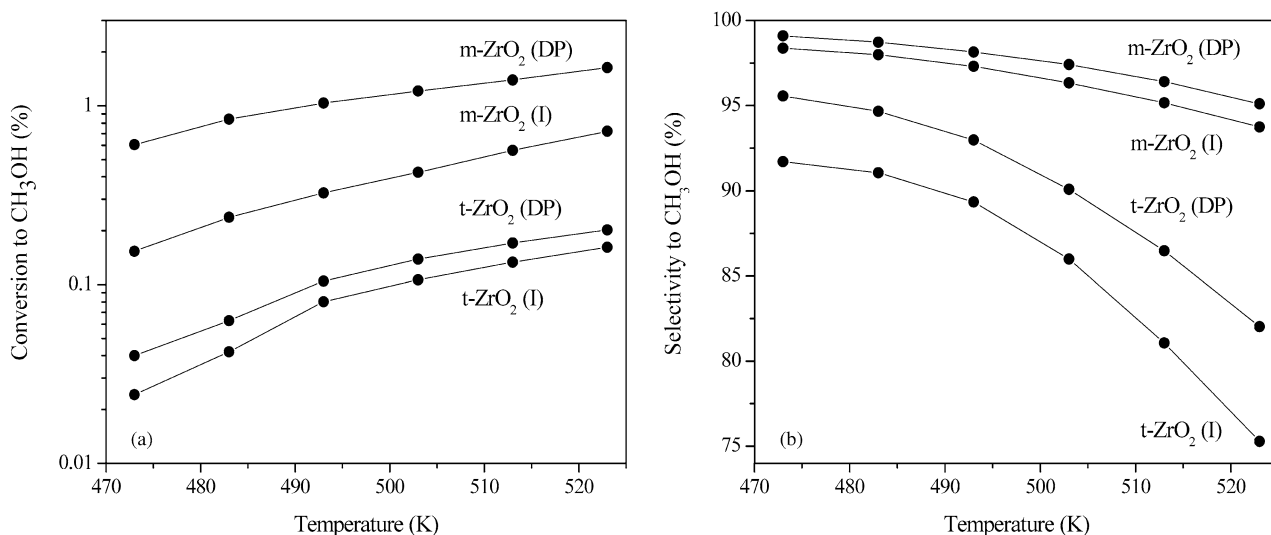


Fig. 7. Effect of temperature on the conversion of CO to methanol (a) and the methanol selectivity (b) during CO hydrogenation over 1.2 wt% Cu/t-ZrO₂ catalysts: catalyst mass = 0.15 g; $P = 3.0$ MPa; $H_2/CO = 3$; total flow rate = $60 \text{ cm}^3/\text{min}$.

Table 4
Effect of increased Cu loading on Cu/m-ZrO₂ on the dispersion of Cu and exchangeable H

Sample	Cu surface area ($\text{m}^2/\text{g}_{\text{cat}}$)	Cu dispersion (%)	Exchangeable H ($\mu\text{mol}/\text{m}^2$)	$-\Delta\text{OH}/\Delta\text{Cu}$ (%)
1.2 wt% Cu/m-ZrO ₂ (DP)	0.87	11.1	10.9	–
6.4 wt% Cu/m-ZrO ₂ (DP)	2.46	5.9	8.2	47
10.0 wt% Cu/m-ZrO ₂ (DP)	2.70	4.2	7.4	33
20.0 wt% Cu/m-ZrO ₂ (DP)	1.88	1.4	6.3	10

in copper loading also results in a monotonic decrease in the concentration of exchangeable hydrogen. This trend is attributable to the adsorption of Cu at surface hydroxyl sites upon deposition [54–57]. Such exchange predominates at lower copper surface densities and facilitates higher levels of dispersion. With increasing copper weight loadings, the relative amount of Cu accommodated at the hydroxyl sites decreases, as illustrated by a decline in the incremental ratio of consumption of hydroxyl groups to copper deposited (last column in Table 4).

The H₂-TPR profile of each catalyst is given in Fig. 8. With larger copper loadings, a greater portion of copper present is reduced at progressively higher temperatures. The most notable distinction occurs when the loading is increased from 10 to 20 wt%, for which case the peak at $\sim 553 \text{ K}$ increases significantly and a new large peak appears at $\sim 598 \text{ K}$. Zhou et al. [45] observed a similar high-temperature peak during the reduction of CuO/ZrO₂ at higher Cu weight loadings and ascribed it to the reduction of bulk CuO. The occurrence of this new peak coincides with the decrease in Cu surface area and a corresponding decrease in Cu dispersion (see Table 4). For each sample, the amount of H₂ consumed was approximately equivalent to the value required for complete reduction of CuO, indicating that the reduction conditions utilized before reaction were sufficient to reduce the copper to metallic Cu.

A comparison of the CO-TPD spectra for 1.2 wt% Cu/m-ZrO₂ (DP) and 10 wt% Cu/m-ZrO₂ (DP) is presented in

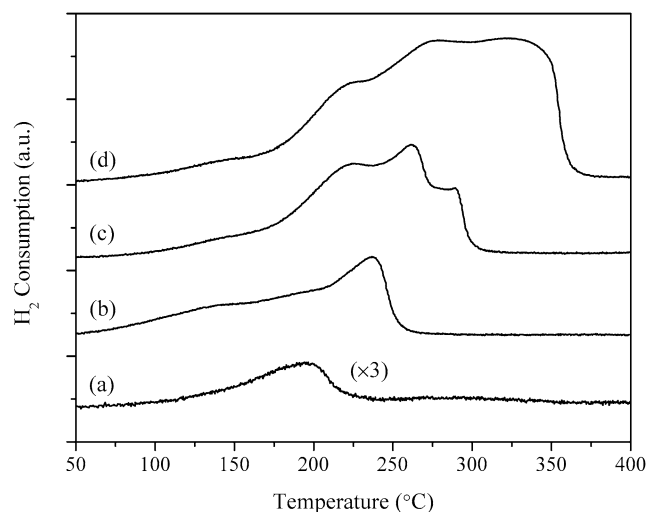


Fig. 8. H₂-TPR spectra for each 1.2 wt% Cu/m-ZrO₂ (DP) catalyst. Heating rate = $20 \text{ K}/\text{min}$; $2\% \text{ H}_2/\text{He}$ flow rate = $60 \text{ cm}^3/\text{min}$. (a) 1.2 wt% Cu, (b) 6.4 wt% Cu, (c) 10 wt% Cu, (d) 20 wt% Cu.

Fig. 9. The two samples exhibited similar desorption spectra for CO and CO₂, with the exception of a small CO peak detected at $\sim 353 \text{ K}$ on 10 wt% Cu/m-ZrO₂ (DP). This peak was also observed in the TPD spectra of other high-weight-loaded samples. Although He et al. [58] have assigned a low-temperature CO-TPD peak for m-ZrO₂ to weakly adsorbed CO, the absence of this peak in the spec-

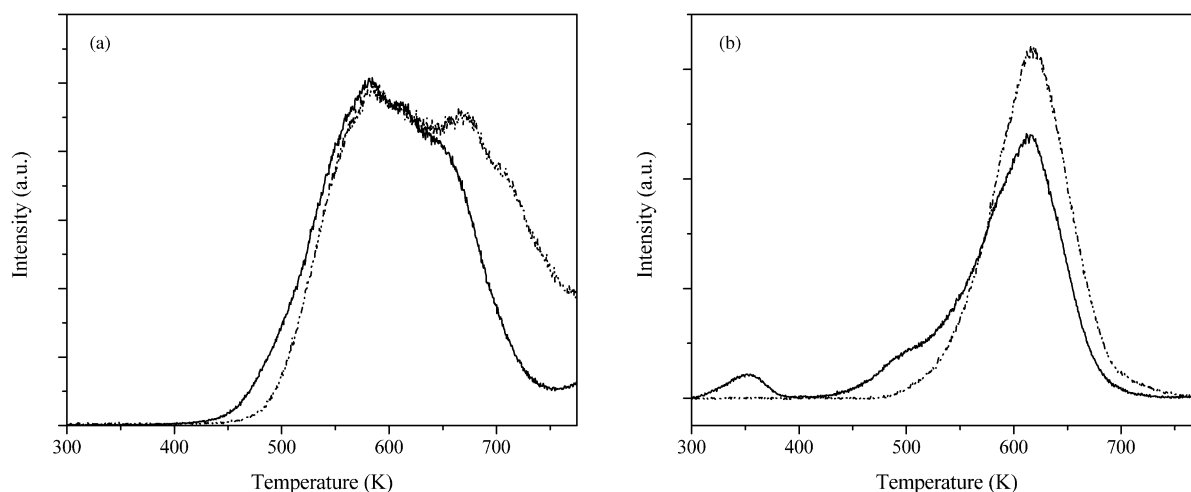


Fig. 9. TPD spectra of (a) CO₂ and (b) CO following CO adsorption on 1.2 wt% Cu/m-ZrO₂ (DP) and 10.0 wt% Cu/m-ZrO₂ (DP). Heating rate = 20 K/min; He flow rate = 60 cm³/min.

Table 5
Effect of increased Cu loading on m-ZrO₂ on the adsorption capacity and binding strength of CO at 523 K

Sample	CO desorption at low <i>T</i> /high <i>T</i> (μmol/m ²)	Peak max. <i>T</i> (K)	CO ₂ desorption (μmol/m ²)	Peak max. <i>T</i> (K)	CO _x desorbed (μmol/m ²)
1.2 wt% Cu/m-ZrO ₂ (DP)	0/0.51	620	0.78	590, 675	1.29
6.4 wt% Cu/m-ZrO ₂ (DP)	0.02/0.39	630	0.77	595, 660	1.18
10.0 wt% Cu/m-ZrO ₂ (DP)	0.02/0.42	620	0.71	585, 655	1.15
20.0 wt% Cu/m-ZrO ₂ (DP)	0.02/0.21	630	0.48	585, 650	0.71

tra for the low-weight-loaded samples reported here suggests that this peak is due to weakly bound CO adsorbed on large Cu crystallites present at higher copper loadings. The low-temperature shoulder at ~ 623 K on the CO peak observed for 10 wt% Cu/m-ZrO₂ (DP) became more prominent with higher weight loading but was never fully resolved. The calculated desorption quantities and related peak maxima temperatures for all of the m-ZrO₂ (DP) samples are listed in Table 5. Each sample exhibits a CO peak at 618–628 K and a broad pair of CO₂ desorption peaks at 583–593 K and 648–673 K. This indicates that the presence of copper in the range of 1.2–20 wt% does not significantly alter the distribution of binding strengths for CO adsorbed to ZrO₂. The total adsorption capacity, however, decreases slightly from 1.2 to 10 wt% Cu before a more precipitous decline is observed for 20 wt% Cu/m-ZrO₂ (DP).

3.5. Effect of Cu loading on the activity and selectivity of Cu/m-ZrO₂

The CO conversion to methanol increased as the temperature was raised from 473 to 523 K with a parallel decrease in selectivity due to increased methane production for each catalyst, as was observed with the lower-weight-loaded materials. Fig. 10 shows the effects of Cu loading on the activity and selectivity of Cu/m-ZrO₂ (DP) for methanol synthesis at 523 K. The activity of Cu/m-ZrO₂ (DP) passes through a maximum at 10 wt% Cu with increasing Cu loading. This

trend is closely associated with the changes in copper surface area for each sample (see Table 4), as discussed below. It should also be noted that the decrease in catalytic turnover of 20 wt% Cu/m-ZrO₂ (DP) coincides with a significant decrease in the concentration of adsorbed CO (see Table 5). Selectivities for each catalyst are quite similar and show only a slight decrease with increasing copper loadings.

4. Discussion

The results of this study demonstrate that both Cu/t-ZrO₂ and Cu/m-ZrO₂ catalysts are active for CO hydrogenation to methanol. Since the surface area of the dispersed Cu influences the methanol synthesis activity, as well as the phase of ZrO₂, it is useful to examine a plot of methanol productivity as a function of Cu surface area for each catalyst. Fig. 11 shows very clearly the strong effect of ZrO₂ phase on activity for a given copper surface area. This plot also demonstrates that for a given phase of ZrO₂, the activity increases linearly with increasing Cu surface area, regardless of whether Cu is introduced by incipient-wetness impregnation or deposition-precipitation. These observations support the idea previously proposed by Bell and co-workers [9,11] that methanol synthesis on Cu/ZrO₂ involves both components, not just Cu. As noted in the Introduction, previous mechanistic investigations have shown that ZrO₂ adsorbs CO, whereas Cu adsorbs H₂ dissociatively and supplies H

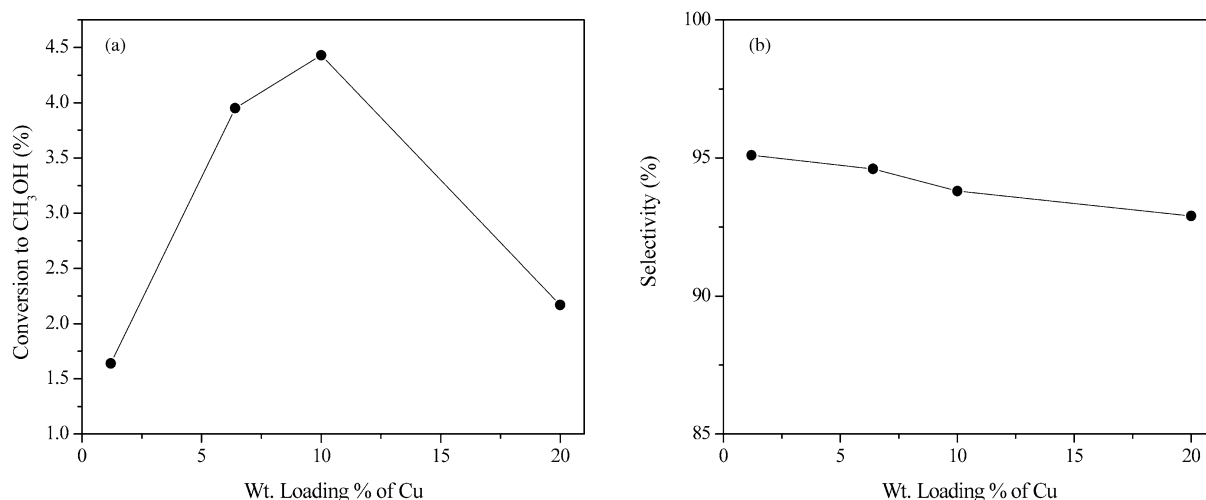


Fig. 10. Effects of Cu loading on the conversion of CO to methanol (a) and the methanol selectivity (b) during CO hydrogenation over Cu/m-ZrO₂: catalyst mass = 0.15 g; $T = 523$ K; $P = 3.0$ MPa; $H_2/CO = 3$; total flow rate = 60 cm³/min.

atoms to ZrO₂ via spillover [9,11,13]. Methanol is formed via the hydrogenation of the adsorbed CO by H atoms migrating from the dispersed Cu particles. Implicit in this interpretation is the assumption that the dispersed Cu is inactive for methanol synthesis from CO/H₂. This assumption is strongly supported by the observation that the (100) surface of Cu exhibits no measurable activity for methanol synthesis from CO and H₂ [59]. Other authors have proposed a similar bifunctional mechanism for methanol synthesis from CO and H₂ on Cu/ZnO catalysts [60,61].

Comparison of the methanol synthesis activity of the Cu/ZrO₂ catalysts prepared in this study with that of a typical industrial catalyst, Cu/ZnO/Al₂O₃, is not easily done, since the performance of the latter class of catalysts depends on the manner of preparation. A further complication is that reports of Cu/ZnO/Al₂O₃ performance often differ in the reaction conditions used (i.e., feed composition, total pressure, reaction temperature) but do not provide sufficient data to permit adjustment of the reported rates and selectivity to a common set of reaction conditions. It is possible, however, to compare the results of the catalysts reported here with the performance of a Cu/ZnO/Al₂O₃ catalyst reported by Lee et al. [12], since the reaction conditions used for catalyst evaluation were identical to those employed here. Those authors prepared a catalyst with the composition CuO/ZnO/Al₂O₃ = 49/36/15 (wt%), which had a BET surface area of 35 m²/g and a Cu surface area of 5.3 m²/g. The methanol synthesis activity of this catalyst operating with a feed of H₂/CO = 3:1 at 523 K and 30 bar was 0.4 μmol/(g s). This activity is essentially identical to that reported here for 1.2 wt% Cu/t-ZrO₂ (DP). For the same reaction conditions, the activity of Cu/m-ZrO₂ ranges from 1.1 to 3.0 μmol/(g s), depending on the surface area of the dispersed Cu (0.8–2.7 m²/g).

The difference in the catalytic activities of Cu/t-ZrO₂ and Cu/m-ZrO₂ parallels the differences in the CO adsorption capacities for these materials at reaction temperature. After CO adsorption for 20 min, the CO adsorption capacity

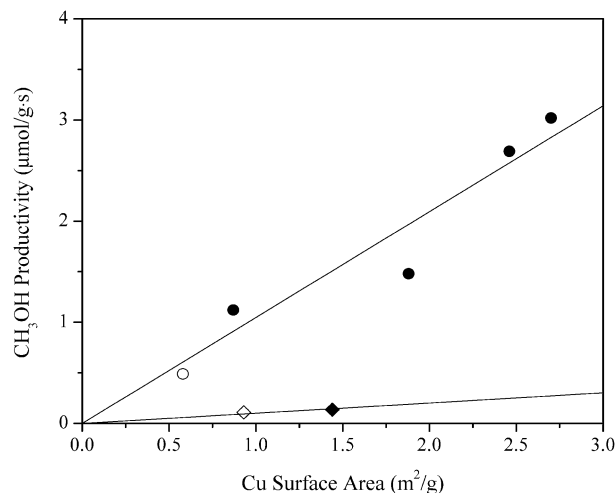


Fig. 11. Methanol productivity versus Cu surface area for each Cu/ZrO₂ catalyst (t-ZrO₂, \diamond ; m-ZrO₂, \blacklozenge ; impregnation, \circ ; deposition-precipitation, \bullet): catalyst mass = 0.15 g; $T = 523$ K; $P = 3.0$ MPa; $H_2/CO = 3$; total flow rate = 60 cm³/min.

of Cu/m-ZrO₂ is approximately 20 times higher at 523 K than that for similarly prepared Cu/t-ZrO₂ (see Table 3). This suggests that at least a part of the reason for the higher activity of Cu/m-ZrO₂, for a given Cu surface area, is the higher concentration of CO and other carbon-containing intermediates on the surface of ZrO₂. A similar observation has been reported by Maruya et al. [20], who noted that the rate of isobutene synthesis from CO and H₂ on ZrO₂ increased with increasing volume fraction of monoclinic ZrO₂, as did the concentrations of formate and methoxide species. Although an increase in the surface concentration of carbon-containing species is expected to contribute to the higher rate of methanol synthesis over Cu/m-ZrO₂, it is not clear whether the phase of ZrO₂ also affects the rate coefficients for the elementary processes involved in the hydrogenation of CO. This subject is addressed in the second paper in this

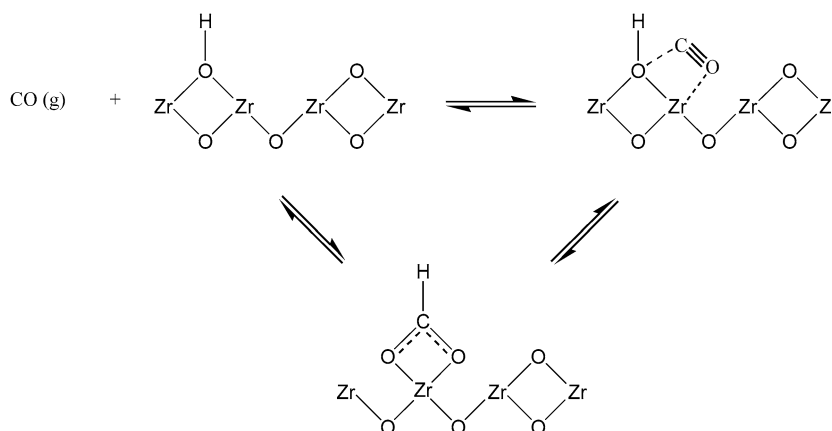


Fig. 12. Proposed mechanism for the formation of formate species at the site of an oxygen vacancy (adopted from Ref. [63]).

series [62]. The balance of the present paper addresses the issue of why the adsorption of CO occurs more rapidly and to a greater extent on Cu/m-ZrO₂ than on Cu/t-ZrO₂. The role of Cu surface area in the rate of methanol synthesis is also discussed.

Previous studies have shown that formate species are generated through an interaction of CO with hydroxyl groups present on ZrO₂ [9,11,54–57]. The infrared spectra presented in Fig. 6 are consistent with this picture, showing that at reaction temperatures CO adsorbs exclusively as bidentate formate species. Although a larger concentration of hydroxyl groups (exchangeable hydrogen) was measured on Cu/m-ZrO₂ (~10.8 μmol/m²) than on Cu/t-ZrO₂ (6.3–7.9 μmol/m²), the difference in hydroxyl group concentration alone is insufficient to account for the higher strength of adsorption and the approximately 20 times larger concentration of adsorbed CO on Cu/m-ZrO₂. In addition, it is unlikely that the hydroxyl groups present on the surface of ZrO₂ are sufficiently acidic to form formate species via direct interaction with CO. This conclusion is supported by theoretical studies which show that the hydroxyl groups on the surface of ZrO₂ are weaker than the Brønsted acid sites of chabazite or the silanol groups on silica [40]. Therefore, it is more likely that the differences in CO adsorption capacity and strength on the two polymorphs of ZrO₂ are due to differences in the local environment of the hydroxyl groups.

In a series of studies on methanol synthesis over ZrO₂, Ekerdt and co-workers [63,64] hypothesized that oxygen vacancies are the active site for CO hydrogenation. The titration of surface anion vacancies with SO₃ demonstrated that predominantly monoclinic ZrO₂ exhibited a significantly greater number of such sites relative to t-ZrO₂ or even c-ZrO₂ materials doped with yttria. This observation is consistent with the detection of Zr³⁺ centers on the surface of m-ZrO₂ by EPR [51,65]. Frost [66] has also proposed that anionic defects are the active centers for CO hydrogenation to methanol on ZnO, ZrO₂, and ThO₂ containing either Cu or other metals.

The proposed scheme for the interaction of CO with a surface oxygen vacancy (adopted from Ref. [63]) is illustrated

in Fig. 12. The vacancy allows a CO molecule to interact with the exposed Zr cations. Formate species are then generated by the reaction of the adsorbed CO with a neighboring hydroxyl group. Based on this picture, the difference in the adsorptive capacity of CO on Cu/t-ZrO₂ and Cu/m-ZrO₂ is expected to be a function of the relative concentration of anionic vacancies present on the surface of the two polymorphs of ZrO₂. Although experimental studies have shown that anionic defects are formed in the bulk and on the surface of ZrO₂, the relative concentrations of such defects on the surface of t- and m-ZrO₂ have not been reported. Embedded cluster calculations give a value of 8.8 eV for the energy required to remove a free O atom from the bulk of t-ZrO₂ [67], whereas plane-wave calculations give a value of 8.88–8.90 eV for the same process occurring in m-ZrO₂ [68]. The energy required to remove an O atom from the low-energy (101) surface of t-ZrO₂ is estimated to be 2.7 [41] and –3.4 eV [67], but unfortunately, a similar estimate has not been made for m-ZrO₂. Consequently, it is not possible to draw a definitive conclusion about the relative ease of forming anionic defects on m-ZrO₂ versus t-ZrO₂ based on theoretical analyses. What is known, however, is that the Lewis acid center produced by the formation of an anionic vacancy strengthens the acidity of an adjacent hydroxyl group [69]. Thus it can be concluded that the formation of O atom vacancies at the surface of ZrO₂ facilitates the reaction of CO with OH groups adjacent to such vacancies and leads to the formation of adsorbed formate species.

Further evidence for the proximity of CO adsorption sites to hydroxyl groups on the surface of ZrO₂ can be drawn from a consideration of the TPD spectra shown in Fig. 5. For both forms of zirconia, adsorbed CO desorbs as both CO and CO₂. As shown in Fig. 13, three possible decomposition pathways can be envisioned [52,70,71]: one leading to the release of CO, and the other two leading to the release of CO₂. The first pathway involves desorption of CO accompanied by regeneration of a hydroxyl group, whereas the second and third pathways involve reaction of the adsorbed formate group with an adjacent hydroxyl group to produce CO₂, accompanied by either a change in the coordi-

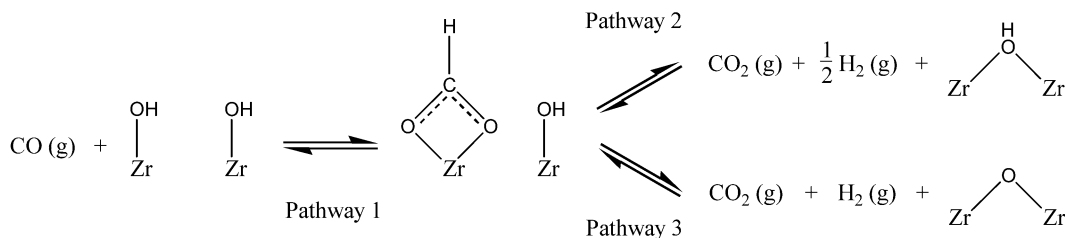


Fig. 13. Proposed pathways for formate decomposition on ZrO_2 .

nation of the hydroxyl group (pathway 2) or dehydroxylation of the oxide (pathway 3). Reaction pathways 2 and 3 both release H_2 . Although some authors [61,72–74] have ascribed the evolution of CO_2 during TPD of adsorbed CO to the decomposition of formate groups on Cu, the presence of a CO_2 desorption peak at the same temperature whether or not Cu is present [17] and the absence of any evidence by infrared spectroscopy for formate species on Cu preclude this interpretation.

The formation of methanol requires a supply of hydrogen atoms for the hydrogenation of formate groups adsorbed to ZrO_2 . Since the heat of reaction needed to form Zr-H and Zr-OH is only -4.1 kcal/mol on defect-free $t\text{-ZrO}_2$ [41], this process is unlikely to provide an adequate supply of atomic hydrogen. H/D exchange studies by Jung and Bell [13] have shown that the rate of H/D exchange occurs much more rapidly on $m\text{-ZrO}_2$ than on $t\text{-ZrO}_2$. Since the latter oxide is believed to have a higher defect density, this leads to the conclusion that anion defects facilitate the dissociation of H_2 . However, even higher rates of H/D exchange are achieved when Cu is deposited on the surface of either ZrO_2 polymorph [11,13]. Fig. 10 shows that for Cu dispersed on both $t\text{-ZrO}_2$ and $m\text{-ZrO}_2$, the rate of methanol formation increases approximately linearly with the surface area of the dispersed Cu. This trend is ascribed to the ability of Cu to adsorb H_2 dissociatively and provide H atoms to ZrO_2 via spillover. Part II of this series [62] presents a detailed transient-response study, aimed at a mechanistic understanding of the intermediates involved in the reaction and their relationship to the mechanism in methanol synthesis. The effect of exposed Cu atoms on the dynamics of CO hydrogenation is also investigated.

5. Conclusions

The activity and selectivity of Cu/ZrO_2 for the synthesis of methanol via CO hydrogenation are influenced strongly by the phase of ZrO_2 . For a given Cu weight loading, $\text{Cu}/m\text{-ZrO}_2$ has an eightfold higher activity for methanol synthesis than $\text{Cu}/t\text{-ZrO}_2$. The selectivity for methanol is also higher on $\text{Cu}/m\text{-ZrO}_2$. For a given phase of ZrO_2 , the methanol synthesis activity increases linearly with increasing Cu surface area. These observations confirm the bifunctional nature of methanol synthesis over Cu/ZrO_2 catalysts. The higher methanol synthesis activity of $\text{Cu}/m\text{-ZrO}_2$ cor-

relates strongly with the higher capacity of this catalyst to adsorb CO as HCOO-Zr species, which are precursors to methanol. It is hypothesized that the higher CO adsorption capacity of $m\text{-ZrO}_2$ is related to a higher concentration of surface anionic vacancies. Such vacancies expose coordinately unsaturated Zr cations and enhance the Brønsted acidity of adjacent Zr-OH groups, which otherwise are only weakly acidic. Thus, the creation of accessible Lewis acid sites in combination with moderately acidic Brønsted acid sites facilitates the adsorption of CO as HCOO-Zr species. In the second part of this study we show that the latter species participate directly in the synthesis of methanol, and that the activity of Cu/ZrO_2 catalysts is related to the surface concentrations of these species.

Acknowledgments

This work was supported by the Director, Office of Basic Energy Sciences, Chemical Sciences Division of the U.S. Department of Energy, under contract DE-AC03-76SF00098.

References

- [1] B. Denise, R.P.A. Sneeden, *Appl. Catal.* 28 (1986) 235.
- [2] Y. Amenomiya, *Appl. Catal.* 30 (1987) 57.
- [3] Y. Nitta, T. Fujimatsu, Y. Okamoto, T. Imanaka, *Catal. Lett.* 17 (1993) 157.
- [4] Y. Sun, P.A. Sermon, *J. Chem. Soc. Commun.* (1993) 1242.
- [5] D. Bianchi, J.L. Gass, M. Khalfallah, S.J. Teichner, *Appl. Catal.* 101 (1993) 297.
- [6] Y. Nitta, O. Suwata, Y. Ikeda, Y. Okamoto, T. Imanaka, *Catal. Lett.* 26 (1994) 345.
- [7] Y. Sun, P.A. Sermon, *Catal. Lett.* 29 (1994) 361.
- [8] I.A. Fisher, H.C. Woo, A.T. Bell, *Catal. Lett.* 44 (1997) 11.
- [9] I.A. Fisher, A.T. Bell, *J. Catal.* 172 (1997) 222; I.A. Fisher, A.T. Bell, *J. Catal.* 178 (1998) 153.
- [10] J. Wambach, A. Baiker, A. Wokaun, *Phys. Chem. Chem. Phys.* 1 (1999) 5071.
- [11] K.T. Jung, A.T. Bell, *Catal. Lett.* 80 (2002) 63.
- [12] J.S. Lee, K.H. Lee, S.Y. Lee, Y.G. Kim, *J. Catal.* 141 (1993) 414.
- [13] K.D. Jung, A.T. Bell, *J. Catal.* 193 (2000) 207.
- [14] C. Morterra, G. Cerrato, L. Ferronia, L. Montanaro, *Mater. Chem. Phys.* 37 (1994) 243.
- [15] V. Bolis, G. Cerrato, G. Magnacca, C. Morterra, *Thermochim. Acta* 312 (1998) 63.
- [16] B. Bachiller-Baeza, I. Rodriguez-Ramos, A. Guerrero-Ruiz, *Langmuir* 14 (1998) 3556.

- [17] K. Pokrovski, K.T. Jung, A.T. Bell, *Langmuir* 17 (2001) 4297.
- [18] Y. Zhao, W. Li, M. Zhang, K. Tao, *Catal. Commun.* 3 (2002) 239.
- [19] S. Ardizzone, C.L. Bianchi, *J. Electroanal. Chem.* 465 (1999) 136.
- [20] K. Maruya, T. Komiya, T. Hayakawa, L. Lu, M. Yashima, *J. Mol. Catal. A: Chem.* 159 (2000) 97.
- [21] D. He, Y. Ding, H. Luo, C. Li, *J. Mol. Catal. A: Chem.* 208 (2004) 267.
- [22] W. Stichert, F. Schüth, S. Kuba, H. Knözinger, *J. Catal.* 198 (2001) 277.
- [23] G.C. Chinchin, K.C. Waugh, D.A. Whan, *Appl. Catal.* 25 (1986) 101.
- [24] G.C. Chinchin, K.C. Waugh, *J. Catal.* 97 (1986) 280.
- [25] K.C. Waugh, *Catal. Today* 15 (1992) 51.
- [26] K.T. Jung, A.T. Bell, *J. Mol. Catal. A: Chem.* 163 (2000) 27.
- [27] J.W. Geus, A.J. van Dillen, in: G. Ertl, H. Knözinger, J. Weitkamp (Eds.), *Preparation of Solid Catalysts*, VCH, Weinheim, 1999, chap. 4.6.
- [28] H. Toraya, M. Yashmura, S. Somiya, *J. Am. Ceram. Soc.* 67 (1984) C-119.
- [29] S. Sato, R. Takahashi, T. Sodesawa, K. Yuma, Y. Obata, *J. Catal.* 196 (2000) 195.
- [30] K.J. Sorenson, N.W. Cant, *Catal. Lett.* 33 (1995) 117.
- [31] R.F. Hicks, C.S. Kellner, B.J. Savatsky, W.C. Hecker, A.T. Bell, *J. Catal.* 71 (1981) 216.
- [32] C. Schild, A. Wokaun, R.A. Koepfel, A. Baiker, *J. Catal.* 130 (1991) 657.
- [33] M. Li, Z. Feng, G. Xiong, P. Ying, Q. Xin, C. Li, *J. Phys. Chem. B* 105 (2001) 8107.
- [34] C. Li, M. Li, *J. Raman Spectrosc.* 33 (2002) 301.
- [35] D. Martin, D. Duprez, *J. Phys. Chem. B* 101 (1997) 4428.
- [36] J. Erkelens, Th.H. Rijntjes, S.H. Eggink-Du Burck, *Recueil* 91 (1972) 1426.
- [37] P.A. Agron, E.L. Fuller, H.F. Holmes, *J. Colloid Interface Sci.* 52 (1975) 553.
- [38] A. Trunschke, D.L. Hoang, H. Lieske, *J. Chem. Soc., Faraday Trans.* 91 (1995) 4441.
- [39] A.A. Tsyganenko, V.N. Filmonov, *J. Mol. Struct.* 19 (1973) 579.
- [40] F. Haase, J. Sauer, *J. Am. Chem. Soc.* 120 (1998) 13503.
- [41] A. Hofmann, S.J. Clark, M. Oettel, I. Hahndorf, *Phys. Chem. Chem. Phys.* 4 (2002) 3500.
- [42] I.M. Iskandarova, A.A. Knizhnik, E.A. Rykova, A.A. Bagatur'yants, B.V. Potopkin, A.A. Korkin, *Microelectron. Eng.* 69 (2002) 587.
- [43] A. Eicheler, G. Kresse, *Phys. Rev. B* 69 (2004) 045402.
- [44] M. Shimokawabe, H. Asakawa, N. Takezawa, *Appl. Catal.* 59 (1990) 45.
- [45] R. Zhou, T. Yu, X. Jiang, F. Chen, X. Zheng, *Appl. Surf. Sci.* 148 (1999) 263.
- [46] D.L. Hoang, H. Lieske, *Catal. Lett.* 27 (1994) 33.
- [47] M.Y. He, J.G. Ekerdt, *J. Catal.* 87 (1984) 381.
- [48] J. Kondo, H. Abe, Y. Sakata, K. Maruya, K. Domen, T. Onishi, *J. Chem. Soc., Faraday Trans.* 1 84 (1988) 511.
- [49] W. Hertl, *Langmuir* 5 (1989) 96.
- [50] C. Schild, A. Wokaun, A. Baiker, *J. Mol. Catal.* 63 (1990) 243.
- [51] E. Guglielminotti, *Langmuir* 6 (1990) 1455.
- [52] D. Bianchi, T. Chafik, M. Khalfallah, S.J. Teichner, *Appl. Catal. A: Gen.* 105 (1993) 223.
- [53] H. Kalies, P. Pinto, G.M. Pajonk, D. Bianchi, *Appl. Catal. A: Gen.* 202 (2000) 197.
- [54] Y. Okamoto, H. Gotoh, *Catal. Today* 36 (1997) 71.
- [55] Y. Okamoto, H. Gotoh, H. Aritani, T. Tanaka, S. Yoshida, *J. Chem. Soc., Faraday Trans.* 93 (1997) 3879.
- [56] V. Indovina, M. Occhiuzzi, D. Pietrogiamici, S. Tuti, *J. Phys. Chem. B* 103 (1999) 9967.
- [57] X. Mugniery, T. Chafik, M. Primet, D. Bianchi, *Catal. Today* 52 (1999) 15.
- [58] M.Y. He, J.M. White, J.G. Ekerdt, *J. Mol. Catal.* 30 (1985) 415.
- [59] J. Nerlov, I. Chorkendorff, *J. Catal.* 181 (1999) 271.
- [60] J. Saussey, J.C. Lavalley, *J. Mol. Catal.* 50 (1989) 343.
- [61] S. Fujita, M. Usui, H. Ito, N. Takezawa, *J. Catal.* 157 (1995) 403.
- [62] M.J. Rhodes, K.A. Pokrovski, A.T. Bell, *J. Catal.* 233 (2005) 210.
- [63] N.B. Jackson, J.G. Ekerdt, *J. Catal.* 101 (1986) 90.
- [64] R.G. Silver, C.J. Hou, J.G. Ekerdt, *J. Catal.* 118 (1989) 400.
- [65] C. Morterra, E. Giamello, L. Osio, M. Volante, *J. Phys. Chem.* 94 (1990) 3111.
- [66] J.C. Frost, *Nature* 334 (1988) 577.
- [67] A.A. Safanov, A.A. Bagatur'yants, A.A. Korkin, *Microelectron. Eng.* 69 (2003) 629.
- [68] A.S. Foster, V.B. Salimov, T. Lopez Gejo, A.L. Shluger, R.M. Nieminen, *Phys. Rev. B* 64 (2001) 244108.
- [69] N.O. Gonzales, A.K. Chakraborty, A.T. Bell, *J. Phys. Chem. B* 101 (1997) 10058.
- [70] M.Y. He, J.W. White, *J. Catal.* 30 (1985) 415.
- [71] S. Takafumi, Y. Iwasawa, *J. Catal.* 129 (1991) 343.
- [72] M. Bowker, R.A. Hadden, H. Houghton, J.N.K. Hyland, K.C. Waugh, *J. Catal.* 109 (1988) 263.
- [73] W.R.A.M. Robinson, *J. Mol. Catal. A: Gen.* 98 (1993) 81.
- [74] B. Sakakini, J. Tabatabaei, M.J. Watson, K.C. Waugh, F.W. Zemicael, *Faraday Discuss.* 105 (1996) 369.